Production cross section measurements of proton-induced reactions on Nb at energies of 58 to 100 MeV

M. Bakhtiari[1] L. Mokhtari Oranj,[2,*] N. S. Jung[2] and H. S. Lee[1,2,†]
[1]*Division of Advanced Nuclear Engineering, POSTECH, Pohang 37673, Republic of Korea*
[2]*Pohang Accelerator Laboratory, POSTECH, Pohang 37673, Republic of Korea*

(Received 25 February 2021; revised 22 May 2021; accepted 15 June 2021; published 29 June 2021)

Production cross sections for the ^{93}Nb$(p,x)^{90}$Mo, ^{92m,90,89m}Nb, ^{89,88,86}Zr, and ^{88,87m,87g}Y reactions were measured using a stacked-foil technique in the proton energy range of 58–100 MeV. The target was arranged in the stack including Nb, Al, Au foils, and Pb plates and was irradiated with 100-MeV protons. After the irradiation, the production yields of the interested radionuclei were measured by a γ-ray spectroscopy system using HPGe detectors. Proton beam intensities were measured using the ^{27}Al$(p,3pn)^{24}$Na, ^{197}Au$(p,p3n)^{194}$Au, and ^{197}Au$(p,pn)^{196}$Au monitor reactions. Some 54 cross section data points were measured, including independent and cumulative cross sections and were compared with other experimental data. The excitation functions of the reactions were also calculated by nuclear models using the TALYS code with a default mode as well as different nuclear level-density models. The calculated cross sections were compared to the measured data and to the TENDL library. It was figured out that the theoretical calculations could reproduce the shape of the measured cross sections well, whereas the magnitude of the cross sections was not reproduced. It was also shown that the preequilibrium mechanism played an important role in the cross section calculations in this paper.

DOI: 10.1103/PhysRevC.103.064617

I. INTRODUCTION

Niobium alloys play an important role in different practical fields, such as accelerator applications. Niobium is used in the coil windings of superconducting magnets as it can withstand high magnetic fields [1]. In addition, high-purity niobium is a preferred material used in the superconducting cavity of particle accelerators due to its high accelerating gradient [2]. The proton-induced reactions are very important in the view of the cavity performance and the radioactivity. Niobium is also used as the target holder and entrance foil in the medical radioisotope production targets, e.g., $H_2\,^{18}O$ irradiated with protons for the ^{18}F production [3]. Furthermore, recently, the ^{93}Nb$(p,4n)^{90}$Mo reaction has drawn the attention of the researchers as a candidate for monitor reactions at proton energies above 40 MeV [4]. The monitor reactions are important in the cross section measurements [5]. The proton-induced reactions on Nb, on the other hand, result in some radionuclei, such as ^{90}Nb, ^{89,88}Zr, and ^{88}Y which are crucial in medical and biological applications [6,7]. The knowledge of their excitation functions will provide a precise prediction and estimation in the above cases. Other researchers have studied the proton-induced reactions on Nb [1,4,7–17]. However, new cross section measurements are still required to improve the excitation functions of these reactions.

In our previous works, the production cross sections of proton-induced reactions on Bi and Pb were measured [18,19]. In this paper, the measured cross sections of ^{93}Nb$(p,x)^{90}$Mo, ^{92m,90,89m}Nb, ^{89,88,86}Zr, and ^{88,87m,87g}Y are presented over the proton energy of 58–100 MeV. The measured cross sections include isomeric and ground-state reaction cross sections and are compared with other experimental data in the literature.

The nuclear model calculations could be evaluated by the measured cross sections at intermediate proton energies either in their default mode or by switching to other modes or models rather than the default one. The contributions of the compound, preequilibrium, and direct mechanisms are also discussed to explain the possible reasons of the discrepancies between the nuclear model calculations and the measured cross sections. Thus, the excitation functions of the mentioned reactions were compared with the calculated cross sections using the TALYS-1.95 [20] code together with the TALYS evaluated nuclear data library (TENDL-2019) [21]. The TENDL library is based on both the default and the adjusted TALYS calculations. The TALYS code is capable to calculate the isomeric and ground-state cross sections separately so that they can be compared with the measured data. The TALYS-1.95 default mode could not reproduce the measured data in the investigated reactions and, in addition, the knowledge of nuclear level densities (NLDs) plays a leading role in the evaluation of nuclear data [22,23]. Therefore, the calculations were performed using the default models as well as using the phenomenological and microscopic NLD models to find out the NLDs impact on the cross section estimations. Various NLD models, such as microscopic NLDs have been developed beside the conventional Fermi-gas-type formulas. Microscopic NLDs provide energy, spin, and parity

*Present address: Deutsches Elektronen-Synchrotron (DESY), Notkestrasse 85, 22607 Hamburg, Germany.
†Corresponding author: lee@postech.ac.kr

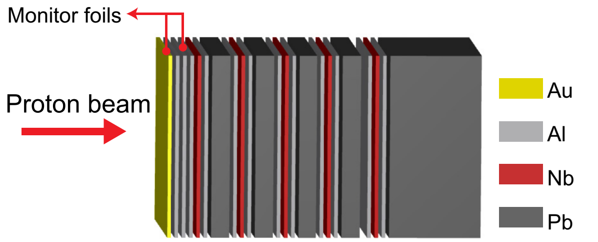

FIG. 1. A schematic of the stacked-foil target.

dependence of NLDs in a nonstatistical way. Such a nonstatistical behavior can have a significant impact on the cross section predictions, particularly, isomeric production cross sections that are known to be sensitive to spin or parity distributions [22,24].

The goal of this paper is to extend the nuclear data libraries for proton-induced reactions on Nb for practical applications and to consider the ability of nuclear model calculations in predicting the reaction cross sections.

II. METHODS

A. Target preparation

The stacked target was irradiated at Korea Multi-purpose Accelerator Complex (KOMAC). A schematic of the target is depicted in Fig. 1 which is similar to our previous works [19,25]. The stack included the Nb activation and monitoring foils that were sandwiched between two Al foils to avoid cross contamination and recoil effects. One Au (30 μm, 19.3 g cm^{-3}, 99.99%) and one Al foil (100 μm, 2.69 g cm^{-3}, 99.99%) were used as the monitoring foils. Natural lead plates were placed between the foils to degrade the proton energy. The thickness of the first four Pb plates was 2 mm and that of the last plate was 10 mm to stop the proton beam. Five Nb foils (50 μm, 8.57 g cm^{-3}, 99.9%) were used as the activation foils. The cross sectional size of the stack was 5$\times$5 cm. All foils were purchased from the Goodfellow Ltd. The amount of major impurities in the Nb samples were 500 ppm of Ta, 100 ppm of W, and less than 10 ppm of Mo [26]. The foils were prepared without any contamination, and their masses were measured using an analytical scale with the precision of 0.1 mg. The total thickness of the target was 1.95 cm which is larger than the range of the 100-MeV proton beam in the target. The required thickness to stop 100-MeV protons in the target was calculated by the SRIM [27] code.

B. γ-ray spectrum and data analysis

The γ-ray spectrum measurement of the activation foils started after cooling time of 30 min. HPGe detectors with relative efficiencies of 15% and 20% were used for γ-ray spectra measurement. The energy resolution of detectors was 1.71-keV full width at half maximum at the 1.33-MeV peak of ^{60}Co. The absolute efficiency of the HPGe detectors were obtained using standard multiline γ-ray sources at positions ranging 10–35 cm from the front face of the detector. Regarding the half-life of a radionuclide, the γ-ray spectra analysis was performed several times, and the averaged cross sections were determined. Canberra's GENIE-2000 (version 3.2) [28], the γ-ray analysis software was used to determine the photopeak area of the γ-ray spectra. For the early γ-ray measurements with a short cooling time, the dead time was about 5% for which the measured cross sections were corrected, and for the later measurements with a longer cooling time, the dead time was less than 1%. Figure 2 shows the typical γ-ray spectra acquired from the Nb sample at two different cooling times after the end of irradiation.

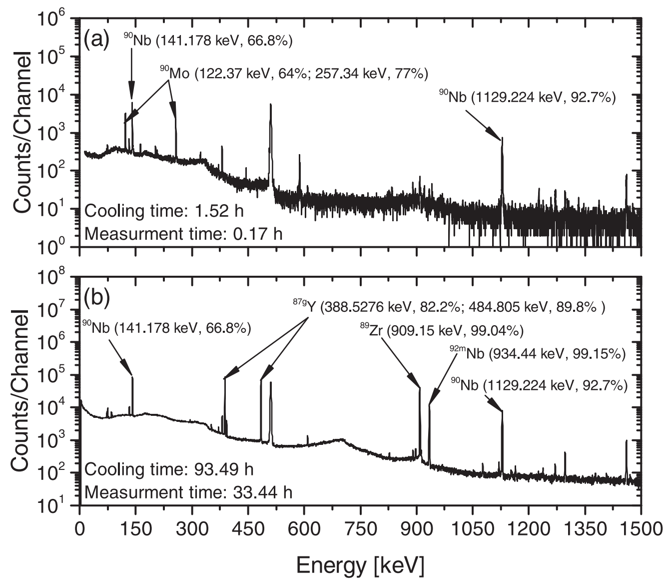

FIG. 2. The γ-ray spectra of the Nb samples (a) 1.52 h after the end of irradiation, and (b) 93.49 h after the end of irradiation.

C. Determination of proton energy and intensity

The stacked foils were irradiated for 45 s by 100-MeV protons with the repetition rate of 1 Hz. The beam shape was described by Gaussian distribution at the target in both x and y directions (z is the beam direction) based on the beam profile measurement using the Gafchromic film [25].

The proton energy striking on each Nb foil was calculated using the SRIM code to be 99.3 ± 0.1, 90.0 ± 0.5, 80.6 ± 0.7, 70.0 ± 0.8, and 58.1 ± 1.2 MeV. The uncertainty of the proton energies on each Nb sample was obtained by considering one standard deviation (1σ) of the transmitted protons through each Nb foil as well as the energy uncertainty in the primary proton beam (0.1 MeV). The contribution of the secondary neutrons and protons to the measured cross sections were negligible.

The proton beam intensity was measured by the activation analysis method using the monitor reactions ^{27}Al$(p,3pn)^{24}$Na, ^{197}Au$(p,pn)^{196}$Au, and ^{197}Au$(p,p3n)^{194}$Au. The production yields of ^{24}Na, ^{196}Au, and ^{194}Au were measured several times by identifying their γ rays listed in Table I and consequently, the average values of their production yields were obtained. Having measured the production yields, and given the number of atoms in the target and the production cross sections of the monitor

TABLE I. Decay characteristic of monitor reactions [30].

Nuclide	Half-life	E_γ (keV)	I_γ (%)	Contributing reactions	Threshold energy (MeV)
^{196}Au	6.1669 ± 0.0006 d	333.03 355.73	22.9 ± 0.9 87 ± 3	^{197}Au(p, pn)	8.11
^{194}Au	38.02 ± 0.1 h	293.548 328.464	10.6 ± 0.15 60.4 ± 0.8	^{197}Au(p, $p3n$)	23.26
^{24}Na	14.997 ± 0.012 h	1368.626 2754.007	99.9936 ± 0.0015 99.855 ± 0.005	^{27}Al(p, $3pn$)	32.6

reactions, the proton beam intensity was measured using the well-known activation equation. The details of the proton beam intensity determination method could be found in Ref. [25]. To obtain the beam intensity, cross sections of the monitor reactions were taken from Refs. [14,29]. The decay data of all radionuclei were taken from Ref. [30] and are listed in Tables I and II. The measured production yields of monitor reactions and relevant proton beam intensities are given in Table III. The uncertainty of the proton beam intensity measurement by the activation analysis was estimated by possible uncertainties of the measured yields (≈2.0%), used cross sections (≈11%), and mass of the monitor activation foils (≈0.01%). The overall uncertainty in the beam intensity measurement was estimated to be approximately 11.4%. For determining the cross sections, the average value of the proton beam intensity was used.

TABLE II. Decay characteristic of measured radionuclei [30].

Nuclide	Half-life	E_γ (keV)	I_γ (%)	Contributing reactions	Threshold energy (MeV)
^{90}Mo	5.56 ± 0.09 h	122.37 257.34	64 ± 3 77 ± 4	^{93}Nb(p, $4n$)^{90}Mo	32.38
^{92m}Nb	10.15 ± 0.02 d	934.44	99.15 ± 0.04	^{93}Nb(p, pn)^{92m}Nb	8.93
		141.178	66.8 ± 0.7	^{93}Nb(p, nt)^{90}Nb	20.5
^{90}Nb	14.6 ± 0.05 h	1129.224	92.7 ± 0.5	^{93}Nb(p, $d2n$)^{90}Nb ^{90}Mo → ^{90}Nb	26.8
^{89m}Nb	66 ± 2 min	507.4 588.0	81 ± 7 95.57 ± 0.13	^{93}Nb(p, $t2n$)^{89m}Nb ^{93}Nb(p, $d3n$)^{89m}Nb ^{93}Nb(p, $p4n$)^{89m}Nb	30.7 37 39.3
^{89}Zr	78.41 ± 0.12 h	909.15	99.04 ± 0.03	^{93}Nb(p, αn)^{89}Zr ^{93}Nb(p, dt)^{89}Zr ^{93}Nb(p, npt)^{89}Zr ^{89}Nb → ^{89}Zr	5.61 23.38 25.63
^{88}Zr	83.4 ± 0.3 d	392.87	97.29 ± 0.09	^{93}Nb(p, $\alpha 2n$)^{88}Zr ^{93}Nb(p, $2t$)^{88}Zr ^{93}Nb(p, ndt)^{88}Zr ^{88}Nb → ^{88}Zr	15.02 26.48 32.8
^{86}Zr	16.5 ± 0.1 h	242.8	95.84 ± 0.2	^{93}Nb(p, $\alpha 4n$)^{86}Zr ^{93}Nb(p, $2n2t$)^{86}Zr ^{93}Nb(p, $3ndt$)^{86}Zr ^{93}Nb(p, $4npt$)^{86}Zr ^{86}Nb → ^{86}Zr	37.1 48.52 54.84 57.1
^{88}Y	106.627 ± 0.021 d	898.042 1836.063	93.7 ± 0.3 99.2 ± 0.3	^{93}Nb(p, αd)^{88}Y ^{93}Nb(p, αpn)^{88}Y ^{93}Nb(p, $t\,^{3}$He)^{88}Y ^{93}Nb(p, pdt)^{88}Y ^{88}Zr → ^{88}Y	11.3 13.55 25.78 31.33
^{87m}Y	13.37 ± 0.03 h	380.79	78.05 ± 0.07	^{93}Nb(p, αt)^{87m}Y ^{93}Nb(p, αdn)^{87m}Y ^{93}Nb(p, $\alpha 2np$)^{87m}Y ^{93}Nb(p, $p2t$)^{87m}Y ^{87}Zr → ^{87m}Y	14.43 20.76 23 34.46
^{87g}Y	79.8 ± 0.3 h	388.5276 484.805	82.2 ± 0.7 89.8 ± 0.9	Same as above ^{87m}Y → ^{87g}Y	14.43

TABLE III. Measured yields of monitor reactions together with measured proton beam intensities.

Method	Reaction	Irradiation time (s)	Production yield (Bq)	Beam intensity (protons/s)
Activation analysis	^{27}Al(p, 3pn)^{24}Na	45	4037.3 ± 68.7	$(9.84 \pm 0.11) \times 10^{11}$
	^{197}Au(p, pn)^{196}Au		1338.8 ± 54.1	$(1.03 \pm 0.11) \times 10^{12}$
	^{197}Au(p, $p3n$)^{194}Au		4614.3 ± 97.6	$(1.03 \pm 0.11) \times 10^{12}$

D. Nuclear model calculations

Theoretical excitation functions were calculated using the TALYS-1.95 [20] code. TALYS is a nuclear model calculation code in which photons, neutrons, protons, deuterons, ^{3}He, and ^{4}He can be used as projectiles in the energy range of 1 keV to 200 MeV for target elements with mass of 12 and heavier [20].

As default, the TALYS code uses the constant temperature model (CTM) [31] at low energies and the Fermi gas model (FGM) [32] at higher energies for NLDs, global optical model potential (OMP) of Koning and Delaroche [33] for OMPs, and it uses γ-ray transmission coefficients, which are generated with the Kopecky-Uhl generalized Lorentzian for the γ-ray strength functions (γSFs) [34]. Preequilibrium reactions that become far more dominant at energies higher than around 10 MeV are modeled according to the two-exciton model [20]. It is known that the nuclear cross sections are dependent on NLDs, OMPs, and γSFs [35–37]. In the Hauser-Feshbach model [38], (A) spin parity of the target and residual nuclei, (B) transmission coefficients of outgoing particles, and (C) photon transmission coefficients are the main ingredients. In the TALYS code, spins and parities could be read from a table or calculated using a NLD model, transmission coefficients of particles are calculated by means of the OMP, and photon transmission coefficients are obtained from the γSF models. In Refs. [39,40], we considered the effects of TALYS nuclear models on reaction cross sections. Moreover, in our previous works [18,19], it was concluded that NLDs were the most effective nuclear ingredients to the reaction cross sections for proton-induced reactions on Bi and Pb. In this paper, the effects of level-density models are studied for the Nb target.

The NLD models used in the TALYS code including phenomenological and microscopic NLD models are listed in Table IV. The results of these models are compared with the measured data and are discussed in Sec. III.

III. RESULTS AND DISCUSSION

The measured independent and cumulative cross section values and their uncertainties are listed in Table V. The excitation functions of the investigated radionuclei are illustrated in Figs. 3–11 including other existing measured data as well as the theoretical calculations. Cross-section values were determined using the standard activation equations. Uncertainties of the presented cross sections were estimated as the sum in quadrature of possible individual uncertainties including proton beam intensity (11.4%), nuclear data (0.03%–4%), detection efficiency (≈1%), net area uncertainty (<2.5%), and sample mass (0.01%). Overall uncertainties were ≈11.5%–12.4%. Uncertainties of measured independent cross sections of ^{90}Nb and ^{88}Y do not include the uncertainties from the decay process of their parent nuclei.

A. ^{93}Nb(p, 4n)^{90}Mo reaction

^{90}Mo ($T_{1/2} = 5.56$ h) decays to ^{90}Nb via electron capture [(EC), 100%]. The 122.37- and 257.34-keV γ rays were used to determine the ^{90}Mo yields. The intense γ rays from ^{90}Mo are located around the peak of the detection efficiency curve, and the measured detection efficiencies could result in a change in the measured cross section values. Figure 3 shows the measured cross sections for the reaction ^{93}Nb(p, 4n)^{90}Mo compared to other experimental data as well as the nuclear model calculations. The cross sections of this reaction were measured by Voyles *et al.* [4], Titarenko *et al.* [11], and Ditrói and co-workers [1,7]. It is seen that our measured data are consistent with the data measured by Titarenko *et al.* [11] and are lower than those of Voyles *et al.* [4].

The TALYS calculations are also illustrated in Fig. 3 using the default mode as well as different NLDs. The general shape of the theoretical calculations agree with the measured data. However, the TALYS default results are shifted down in energy by almost 7 MeV. LDM-5 and LDM-6 show reasonable threshold energies, whereas they underestimate the measured data at the peak. LDM-2 indicates the similar cross section magnitude to the measured data by Titarenko *et al.* [11]. On the other hand, LDM-4 seems to be in agreement with the data in the present paper from 70 to 100 MeV, overestimating other experimental data around 50 MeV. LDM-3 shows very low cross sections. The TENDL data also underestimate the

TABLE IV. Different nuclear level-density models implemented in the TALYS code.

Phenomenological	Microscopic
Default: CTM [31]+FGM [32]	LDM-4: Microscopic level densities on the basis of Hartree-Fock calculations [41]
LDM-2: Backshifted Fermi gas model [32]	LDM-5: Hilaire and Goriely microscopic combinatorial model [24]
LDM-3: Generalized superfluid model [42]	LDM-6: Microscopic level densities based on temperature-dependent Hartree-Fock-Bogoliubov [22]

TABLE V. Measured cross sections of Mo, Nb, Zr, and Y radioisotopes produced from the ^{93}Nb(p, x) reactions. "Ind" and "Cum" stand for independent and cumulative cross sections, respectively.

		$\sigma \pm \Delta\sigma$ (mb)				
Nuclide	E_p (MeV)	99.3 ± 0.1	90.0 ± 0.5	80.6 ± 0.7	70.0 ± 0.8	58.1 ± 1.2
^{90}Mo$^{\text{Ind}}$		9.3 ± 1.1	11.6 ± 1.4	15.1 ± 1.8	19.6 ± 2.3	53.5 ± 6.3
^{92m}Nb$^{\text{Ind}}$		36.7 ± 4.2	42.8 ± 4.9	46.4 ± 5.3	48.5 ± 5.5	52.7 ± 6.0
^{90}Nb$^{\text{Ind}}$		114.6 ± 13.1	125.7 ± 14.4	141.8 ± 16.2	180.9 ± 20.7	305.1 ± 34.9
^{90}Nb$^{\text{Cum}}$		128.5 ± 14.7	143.7 ± 16.5	165.9 ± 19.0	211.9 ± 24.3	389.0 ± 44.6
^{89m}Nb$^{\text{Ind}}$		10.6 ± 1.2	13.5 ± 1.6	15.8 ± 1.9	22.3 ± 2.8	10.7 ± 1.2
^{89}Zr$^{\text{Cum}}$		165.6 ± 18.9	181.5 ± 20.7	212.9 ± 24.3	269.0 ± 30.7	116.5 ± 13.3
^{88}Zr$^{\text{Cum}}$		125.5 ± 14.5	140.5 ± 16.1	128.6 ± 14.7	48.6 ± 5.6	23.6 ± 2.7
^{86}Zr$^{\text{Cum}}$		12.3 ± 1.4	10.0 ± 1.2	14.9 ± 1.7	15.0 ± 1.7	
^{88}Y$^{\text{Ind}}$		18.1 ± 2.1	18.3 ± 2.1	14.9 ± 1.7	9.5 ± 1.1	9.5 ± 1.2
^{87m}Y$^{\text{Cum}}$		96.3 ± 11.3	70.0 ± 8.0	41.8 ± 4.8	51.1 ± 5.9	71.4 ± 8.2
^{87g}Y$^{\text{Cum}}$		117.6 ± 13.5	86.8 ± 9.9	50.1 ± 5.7	59.6 ± 6.8	85.3 ± 9.8

measured cross sections, and they predict the peak position shifted down in the energy. It seems that more cross-section measurements are needed to confirm the shape of the excitation functions over the whole proton energy range for this reaction.

B. ^{93}Nb(p, pn)^{92m}Nb reaction

The isomeric state cross sections of ^{92m}Nb ($T_{1/2} =$ 10.15 d; EC, 100%) were measured. The ground state of ^{92}Nb has a long half-life of 3.47×10^7 yr. Considering that the half-life of the ground state is extremely long, the measured cross sections from short measurements represent only the cross sections of the metastable state. In addition, there is no precursor to decay to ^{92m}Nb so that the measured cross sections are independent cross sections. The production yields were measured using the intense γ ray of 934.44 keV. Because of the suitable half-life of this radionuclide, its production cross sections have been measured by several researchers [1,4,7,9–13]. Figure 4 shows the cross sections of the reaction ^{93}Nb(p, pn)^{92m}Nb measured in this paper and other experimental data. Our measured independent cross sections are in good agreement with the data measured by Voyles *et al.* [4], Titarenko *et al.* [11], Michel *et al.* [14], and Ditrói *et al.* [1]. The TALYS calculations indicate different peaks so that LDM-3 estimates quite high cross-section data. The TALYS defaults, LDM-2, LDM-4, LDM-5, and LDM-6 predict the cross sections at the peak well. However, all NLDs overestimate the experimental cross sections above 40 MeV. The TENDL data show lower values around the peak, however, they are in good

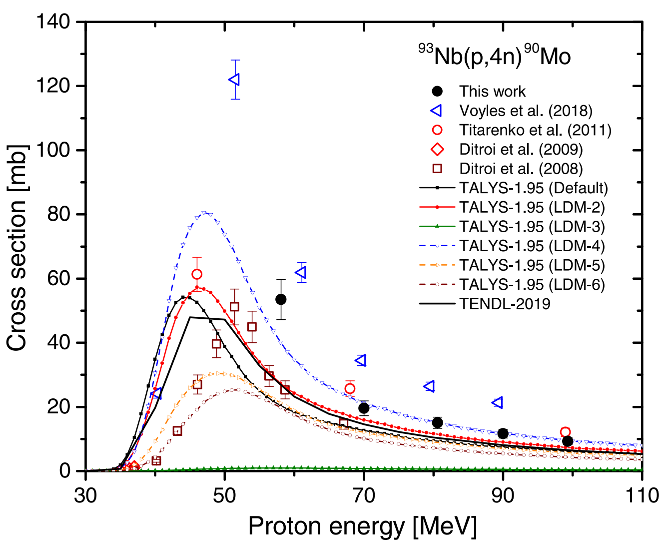

FIG. 3. Measured independent cross sections for the ^{93}Nb($p, 4n$)^{90}Mo reaction compared with the previously published data together with the theoretical calculations based on the TALYS code. The experimental data are taken from Refs. [1,4,7,11].

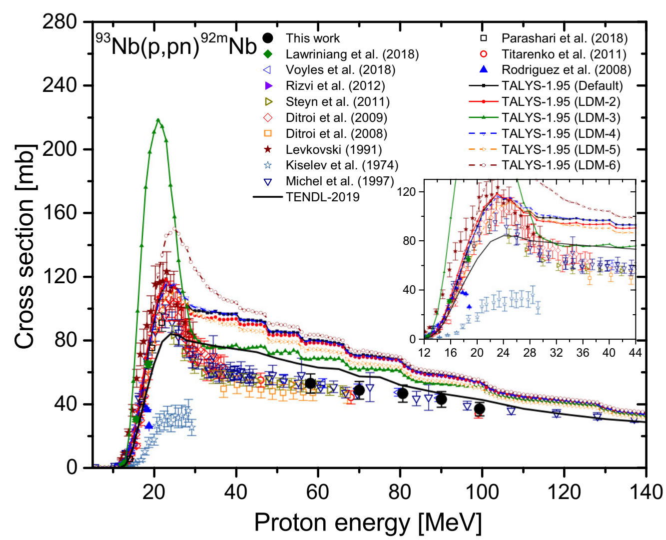

FIG. 4. Measured independent cross sections for the ^{90}Nb($p, 4n$)^{92m}Nb reaction compared with the previously published data together with the theoretical calculations based on the TALYS code. The experimental data are taken from Refs. [1,4,7–16].

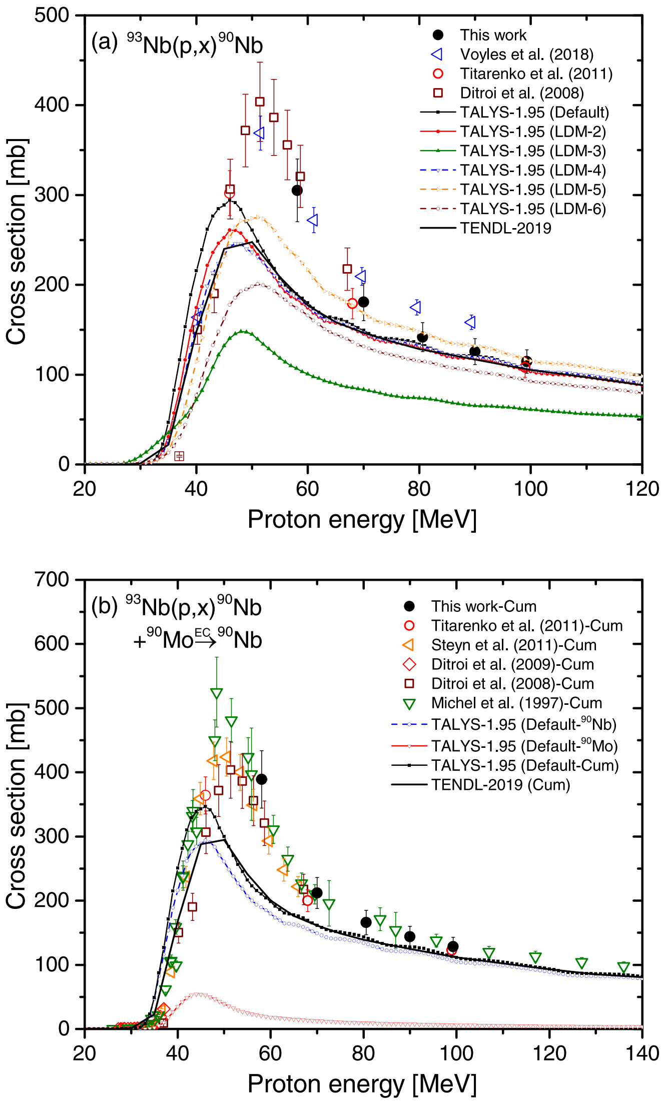

FIG. 5. (a) Measured independent cross sections and (b) measured cumulative cross sections (indicated by "Cum") for the ^{93}Nb$(p, x)^{90}$Nb reaction compared with the previously published data together with the theoretical calculations based on the TALYS code. The experimental data are taken from Refs. [1,4,7,11,12,14].

agreement with the measured data at the high proton energies above 60 MeV. It might be interpreted that the evaluated data from the TENDL library allocate less contributions from the compound mechanism but emphasize the preequilibrium contribution at the higher proton energies.

C. ^{93}Nb$(p, x)^{90}$Nb reaction

^{90}Nb ($T_{1/2} = 14.60$ h; EC, 100%) can be produced through different nuclear reaction channels as well as from the decay of ^{90}Mo (Table II). The cumulative and independent cross sections could be measured. The cross sections of this radionuclide were obtained by identifying 141.178- and 1129.224-keV γ rays.

The independent cross sections are shown in Fig. 5(a) with comparison of other experimental data in the literature as well as the theoretical calculations. The experimental data in the literature were rare and reported by Voyles *et al.* [4], Titarenko *et al.* [11], and Ditrói *et al.* [1]. It can be seen from Fig. 5(a) that measured cross sections in this paper are in good agreement with those of Ditrói *et al.* [1] and Titarenko *et al.* [11]. The experimental data measured by Voyles *et al.* [4] are higher than our measured data. On the other hand, the TALYS calculations reveal the fact that the cross section calculations are highly dependent on the nuclear level density applied in the code. The TALYS defaults, LDM-2 and LDM-4 show the position of the maximum cross section at around 46 MeV, whereas the experimental data present the peak position at 51 MeV. It is seen that LDM-5 shows more reasonable estimation from 70 to 100 MeV. LDM-6 predicts the lowest cross section values among the models. The TENDL cross sections misplace the peak center, and they underestimate both the measured cross sections and the TALYS default calculations.

The cumulative cross sections of ^{90}Nb were also measured and are depicted in Fig. 5(b) together with other experimental data. It is seen that the measured cross sections in the present paper are quite consistent with the data measured in Refs. [11,14]. In the case of the TALYS calculations, the production cross sections of ^{90}Mo and ^{90}Nb are added together in the default mode to obtain the cumulative cross sections to be compared with the experimental data. The TALYS calculations and the TENDL library predict the reaction threshold reasonably and are in agreement with the measured data up to 45 MeV and above 80 MeV. However, they underestimate the data around the peak region.

D. ^{93}Nb$(p, x)^{89m}$Nb reaction

The production yields of the isomeric state of ^{89m}Nb ($T_{1/2} = 5.80$ h) were measured using the intense γ ray of 588 keV. The independent cross sections of this reaction were rare in the investigated proton energy range (Fig. 6). Our measurement results are similar to that of Titarenko *et al.* [11] at 100 MeV. The data measured by Voyles *et al.* [4] are higher than our measurement. The TALYS calculations could predict the reaction threshold well except for LDM-3 that shows a lower threshold. In addition, the theoretical calculations could not reproduce the experimental data over the whole proton energy range, particularly, LDM-5 and LDM-6 underestimate the the cross section data significantly for this isomeric state of ^{89}Nb. The illustrated results from the TENDL library show a deviation from the TALYS default calculations at the threshold up to 65 MeV and after that they are consistent with each other. TENDL underestimates the experimental cross sections significantly. Further experiments seem to be necessary for this reaction.

E. ^{93}Nb$(p, x)^{89}$Zr reaction

The production yields of ^{89}Zr ($T_{1/2} = 78.41$ h) were measured by a 909.15-keV γ ray. As listed in Table II, ^{89}Zr is produced via different nuclear reaction channels depending on the proton energy. In addition, ^{89}Nb decays to ^{89}Zr and because the cross sections of ^{89}Nb could not be obtained, the cumulative cross sections were only measured. Our

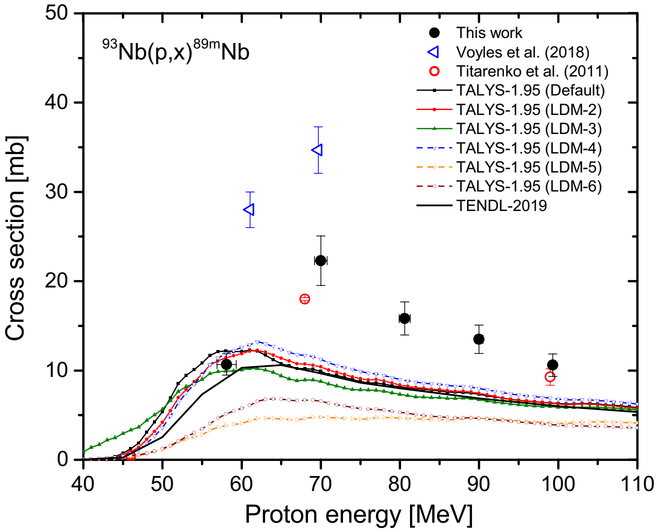

FIG. 6. Measured independent cross sections for the ^{93}Nb$(p, x)^{89m}$Nb reaction compared with the previously published data together with the theoretical calculations based on the TALYS code. The experimental data are taken from Refs. [4,11].

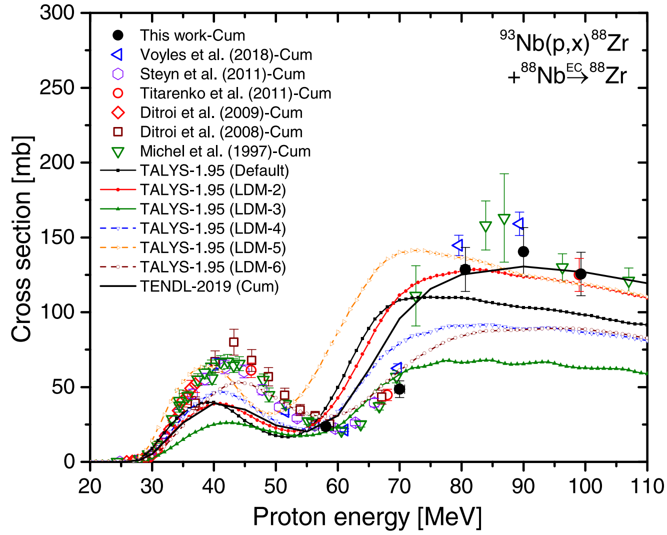

FIG. 8. Measured cumulative cross sections (indicated by Cum) for the ^{93}Nb$(p, x)^{88}$Zr reaction compared with the previously published data together with the theoretical calculations based on the TALYS code. The experimental data are taken from Refs. [1,4,7,11,12,14].

measured data with other experimental data are shown in Fig. 7 together with the theoretical calculations. The present results are consistent with the data measured by Titarenko *et al.* [11] and Steyn *et al.* [12], and are slightly lower than those of Voyles *et al.* [4]. For comparing the TALYS calculations with the experimental data, the cross sections of ^{89}Nb and ^{89}Zr are summed up in the default mode.

In the ^{89}Zr production, the $(p, \alpha n)$ channel is open at the proton energy of 5.6 MeV and it seems that the TALYS calculations could reproduce the measured data well up to 40 MeV. However, as the proton energy increases, other nuclear reaction channels, such as (p, npt) open for which the TALYS results deviate from the experimental data. It can be deduced that in case the composite particles are emitted, the nuclear models can handle the calculations better than the case with separated emitted particles. The TENDL data, however, depict more reasonable estimation of the excitation function shape for this reaction. TENDL presents lower results than the measured data at around 70 MeV.

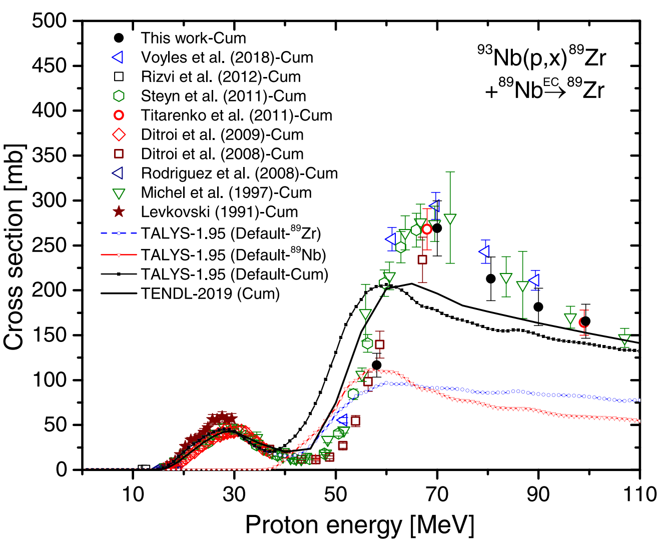

FIG. 7. Measured cumulative cross sections (indicated by Cum) for the ^{93}Nb$(p, x)^{89}$Zr reaction compared with the previously published data together with the theoretical calculations based on the TALYS code. The experimental data are taken from Refs. [1,4,7,9–15].

F. ^{93}Nb$(p, x)^{88}$Zr reaction

The production yields of ^{88}Zr with a long half-life of 83.4 d were measured using its strong γ ray of 392.87. It can be produced via different nuclear reaction channels. The cumulative cross sections are illustrated in Fig. 8. Our results are in good agreement with Ref. [11] and slightly lower than the data reported in Ref. [4].

The theoretical calculations using the default mode and different level-density models are shown as well. Because, the cross sections of parent nuclei ^{88}Nb calculated by the TALYS code were negligible, they are not shown in the figure. It is clearly seen that NLDs have a great impact on the reaction cross sections. This is, particularly, more obvious at proton energies above 50 MeV. All NLDs predict the reaction threshold well and LDM-5 shows the maximum cross section more reasonable than other NLDs however, it overestimates the measured data between 50 and 75 MeV. Generally, LDM-3 and LDM-6 underestimate the measured data. As shown in Table II, the exit channel includes two protons and four neutrons for ^{93}Nb$(p, x)^{88}$Zr reaction so that composite particles, such as α particles could be emitted at lower proton energies. Therefore, the models related to the α particles would play an important role at low proton energies. The theoretical

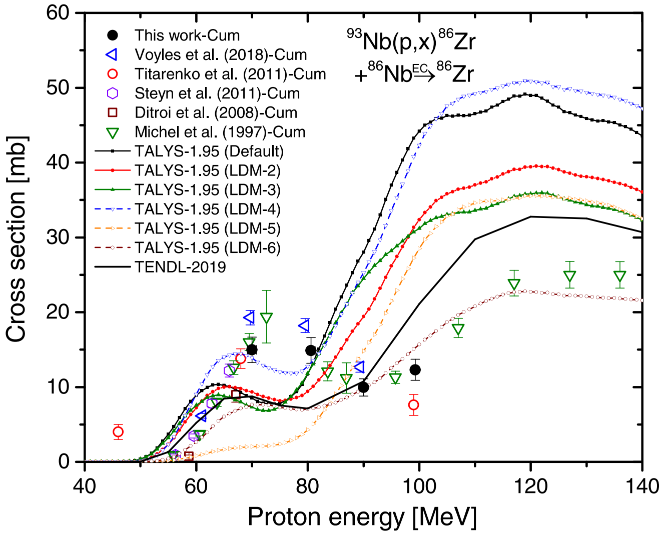

FIG. 9. Measured cumulative cross sections (indicated by Cum) for the ^{93}Nb$(p, x)^{86}$Zr reaction compared with the previously published data together with the theoretical calculations based on the TALYS code. The experimental data are taken from Refs. [1,4,11,12,14].

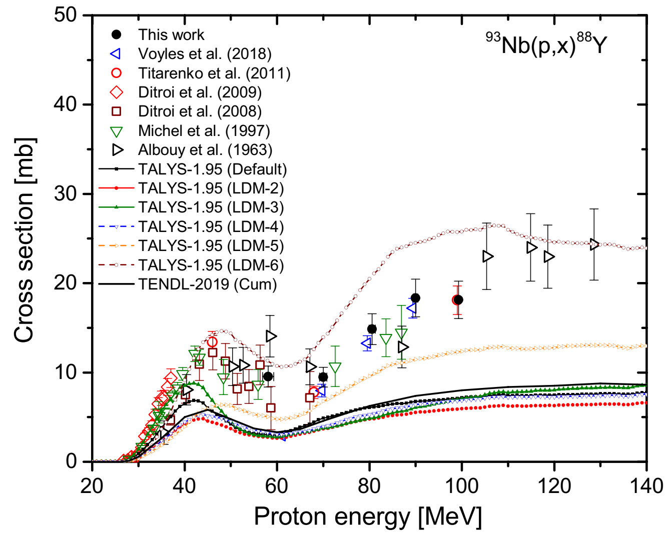

FIG. 10. Measured independent cross sections for the ^{93}Nb$(p, x)^{88}$Y reaction compared with the previously published data together with the theoretical calculations based on the TALYS code. The experimental data are taken from Refs. [1,4,7,11,14,17].

calculations seem to be less in agreement with the measured data at higher proton energies as more nuclear reaction channels containing more separated particles become feasible.

In the case of the TENDL results, it can be seen that they underestimate the first peak of the measured data which is related to the compound mechanism, whereas they are in a good agreement with the measured data at the high proton energies. The high-energy tail is assumed to be related to the preequilibrium mechanism, and it seems that the TENDL library is describing the preequilibrium effects well, whereas the compound part is less consistent with the measured data.

G. ^{93}Nb$(p, x)^{86}$Zr reaction

The production yields of ^{86}Zr ($T_{1/2} = 16.5$ h) were measured by identifying its intense γ ray with energy of 242.8 keV. This nuclei could be produced through several nuclear reaction channels with the minimum reaction threshold energy of 37.22 MeV. It might also be generated from the decay of ^{86}Nb ($T_{1/2} = 88$ s). The results are depicted in Fig. 9 in comparison with other available experimental data. It is seen that our results are in agreement with the data measured by Michel *et al.* [14] and are slightly higher than that of Titarenko *et al.* [11] at 100 MeV. The measured data by Voyles *et al.* [4] are somewhat higher than our data. The TALYS calculations showed a negligible contribution of ^{86}Nb to the excitation functions, thus, are not indicated in the figure. In this reaction, two protons and six neutrons exist in the exit channel which make the reaction much more complicated. At lower threshold energies composite particles are emitted via the ^{93}Nb$(p, \alpha 4n)$ reaction, whereas at higher energies particles tend to be separated so that $(p, 4npt)$ channel opens at around 57 MeV. Regarding Fig. 9, all NLDs could not reproduce the position of the maximum measured cross section value at 75 MeV. However, LDM-5 reproduces the experimental data well from 90 to 140 MeV. Other NLD models overestimate the measured data considerably above 80 MeV. As shown in the figure, the TENDL data reproduce different shape and the magnitude of the measured cross sections for this reaction. However, the TENDL results are smaller than those of the TALYS code.

H. ^{93}Nb$(p, x)^{88}$Y reaction

^{88}Y has an isomeric state with the half-life of 0.301 ms that decays to the ground state via isomeric transition. The 898.042- and 1836.063-keV γ rays from the ground state could be detected for measuring the production yields of ^{88}Y. Several nuclear reaction channels contribute to the formations of ^{88}Y, and it can be fed from the parent ^{88}Zr ($T_{1/2} = 83.4$ d). The independent cross sections were measured and are shown in Fig. 10 with other experimental data and the theoretical calculations. Our results are in good consistency with the data measured by Titarenko *et al.* [11] and Voyles *et al.* [4]. The TENDL data as well as the theoretical calculations by the TALYS code show a reasonable reaction threshold. LDM-6 reproduces the first peak in shape and magnitude, and it overestimates the data from 70 to 100 MeV. It is in an agreement with the data measured by Albouy *et al.* [17] above 100 MeV. Other NLD models underestimate the experimental data above 40 MeV.

I. ^{93}Nb$(p, x)^{87m,87g}$Y reactions

^{87m}Y ($T_{1/2} = 13.37$ h) decays to the ground-state ^{87g}Y ($T_{1/2} = 79.8$ h) via isomeric transition, emitting a 380.79-keV γ ray. The ground state was identified by 388.5276- and 484.805-keV γ rays. The isomeric state could be produced from different nuclear channels as indicated in Table II, and it could be produced from the decay of ^{87}Zr ($T_{1/2} = 1.68$ h) as well.

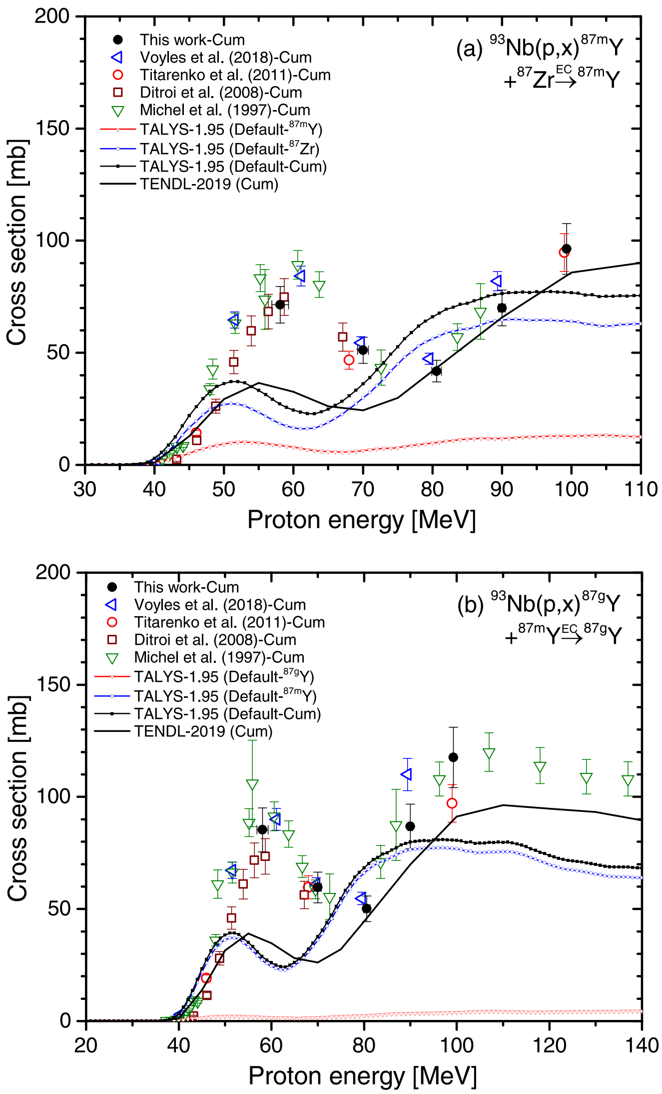

FIG. 11. Measured cumulative cross sections for the (a) ^{93}Nb$(p,x)^{87m}$Y and (b) ^{93}Nb$(p,x)^{87g}$Y reactions compared with the previously published data together with the theoretical calculations based on the TALYS code. The experimental data are taken from Refs. [1,4,11,14].

Because the production cross sections of the ^{87}Zr could not be measured, the measured cross sections of the isomeric and ground sates were cumulative. The results for the isomeric and ground states are indicated in Fig. 11. Our data are in agreement with other experimental data over the whole investigated proton energy range for both the isomeric and the ground states. The TALYS code can calculate the isomeric and ground-state production cross sections separately.

As illustrated in Fig. 11(a), the calculated cumulative cross sections show the reaction threshold quite well, whereas they underestimate the fist peak at around 60 MeV considerably. Above 70 MeV, however, the calculations are in reasonable agreement with the measured data for ^{87m}Y. The TENDL data show the position of the first peak slightly better than the TALYS code, however, it is still mismatched with the experimental data. For the high proton energy region, the TENDL results are in reasonable agreement with the measured data. Similar to the previously discussed reactions, TENDL indicates a better description of the preequilibrium mechanism. On the other hand, the theoretical calculations underestimate the measured data for ^{87g}Y and could not estimate the shape and magnitude of the cross sections at the peaks [Fig. 11(b)]. Although the TENDL data tend to show a better agreement with the measured data particularly around the second peak.

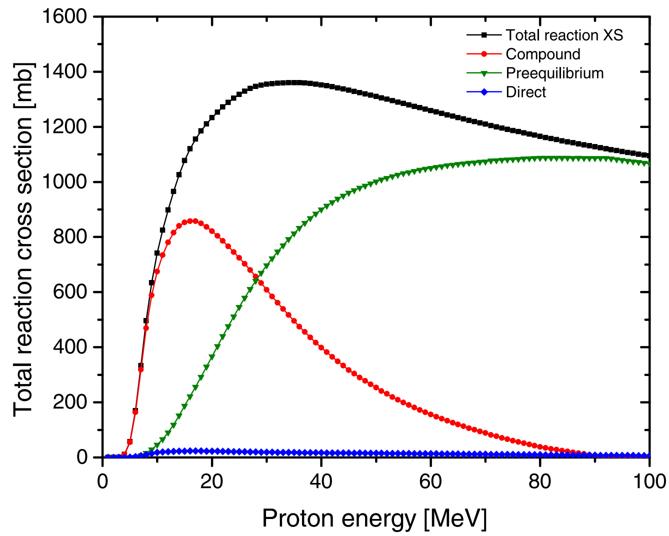

FIG. 12. Contribution of the compound, preequilibrium, and direct mechanisms to the total reaction cross section of the ^{93}Nb(p,x) reaction calculated by the TALYS-1.95 code.

J. Discussion on the nuclear model calculations

In order to explain the disagreement of the theoretical calculations with the measurement, the contribution of different reaction mechanisms to the reaction cross section are shown in Fig. 12. As can be seen from the figure, the contribution of the compound mechanism is dominant at low proton energies, whereas the preequilibrium mechanism takes the lead at higher proton energies. The direct mechanism contribution is negligible. Thus, several reasons might be expected as follows that the calculated cross sections differ from the experimental data. (A) The energy at which the preequilibrium becomes dominant is around 30 MeV, but this value might be higher or lower. An inaccurate estimate of the preequilibrium contribution to the cross section would eventually result to inaccurate compound nucleus cross sections. (B) According to the Hauser-Fechbach formalism, which describes the compound reactions, the important ingredients are the nuclear level densities, optical models, and γ-ray strength functions [9,43]. By assuming more or less contributions of the compound mechanism to the reaction cross sections, the effect of a level-density model becomes more evident. By changing the NLD model, in fact, the level-density parameters are different, resulting in different cross section values. (C) The preequilibrium mechanism is described by the exciton model in the TALYS code [44], and its contribution is dominant at high proton energies. The models and corresponding parameters play a very important role in the cross-section estimation at these energies. (D) In the ^{93}Nb(p, x) reactions, there are many open channels so that the nuclear models might overestimate the cross sections of one channel and, consequently, underestimate another channel cross section. This misprediction of the channels by the code could also be the reason for the disagreement.

As was discussed, the contribution of the preequilibrium mechanism to the cross sections becomes considerable at proton energies above 30 MeV. It seemed that the evaluated data in the TENDL library could describe the preequilibrium mechanism quite well. However, TENDL underestimated the measured data at the lower proton energies which are related to the compound mechanism.

IV. CONCLUSION

The cross sections for the proton-induced reactions on Nb were measured for the ^{93}Nb$(p, x)^{90}$Mo, ^{92m,90,89m}Nb, ^{89,88,86}Zr, and ^{88,87m,87g}Y between 58 and 100 MeV. Some 54 cross section data points were obtained including cumulative and independent cross sections. The measured data also contained the isomeric and ground-state reaction cross sections which are suitable for investigating the nuclear models calculations. Our results were in good agreement with the most experimental data in the literature.

The nuclear model calculations using the TALYS code were also performed using the default mode as well as using various level-density models. The cross sections from the TENDL-2019 library were also taken for the comparison. In general, the TALYS calculations and the TENDL data could reproduce the shape of the measured cross sections well even for ^{89,88,86}Zr with two peaks. However, they could not show the position of the maximum cross sections correctly, and for the most cases, the calculations were shifted down in energy. It was found out that the TALYS code could reproduce the excitation functions at low proton energies well when composite particles, such as α particles are emitted. For the ^{93}Nb$(p, x)^{90}$Mo, ^{92m,90,89m}Nb reactions, all NLDs were unable to predict the position of cross section peak. In the case of ^{93}Nb$(p, x)^{89,88,86}$Zr, ^{88,87m,87g}Y reactions, however, NLDs were in a better agreement with the experimental data at low proton energies, whereas at higher proton energies, the nuclear model calculations deviated from the experimental data significantly. In general, the TENDL library presented smaller cross sections than the TALYS code. It was shown that the TENDL library could reproduce the high-energy tail of the excitation functions better than the TALYS code. The results in this paper showed that existence of several particles in the exit channel makes the cross section calculations more complicated, and the nuclear models need to be improved.

Our measured cross sections can extend the nuclear data for Nb and can be useful for more reliable evaluated cross section data. It was also confirmed that the NLD models, which are related to the compound nucleus, as well as the preequilibrium mechanism play a significant role in the reaction cross section estimation. The NLDs which are implemented in the TALYS code require to be more improved.

ACKNOWLEDGMENTS

We would like to thank the KOMAC team for their cooperation during the experiment. We also thank our colleagues Dr. Y. U. Kye and A. Lee for their help. This work was supported by the Nuclear Safety Research Program through the Korea Foundation of Nuclear Safety (KOFONS), granted financial resources from the Nuclear Safety and Security Commission (NSSC) of Republic of Korea (Grants No. 1303026 and No. 1603005).

[1] F. Ditrói, S. Takács, F. Tárkányi, M. Baba, E. Corniani, and Y. Shubin, Study of proton induced reactions on niobium targets up to 70 MeV, Nucl. Instrum. Methods Phys. Res. Sect. B **266**, 5087 (2008).

[2] X. Singer, E. Filimonova, D. Reschke, A. Rostovtsev, W. Singer, T. Tokareva, and V. Zaharov, Single-cell superconducting RF cavities from ultra-high-purity niobium, Nucl. Instrum. Methods Phys. Res. Sect. A **574**, 518 (2007).

[3] M. S. Berridge, K. W. Voelker, and B. Bennington, High-yield, low-pressure [18O] water targets of titanium and niobium for F-18 production on MC-17 cyclotrons, Appl. Radiat. Isot. **57**, 303 (2002).

[4] A. S. Voyles, L. A. Bernstein, E. R. Birnbaum, J. W. Engle, S. A. Graves, T. Kawano, A. M. Lewis, and F. M. Nortier, Excitation functions for (p,x) reactions of niobium in the energy range of Ep = 40–90 MeV, Nucl. Instrum. Methods Phys. Res. Sect. B **429**, 53 (2018).

[5] A. Hermanne, A. Ignatyuk, R. Capote, B. Carlson, J. Engle, M. Kellett, T. Kibédi, G. Kim, F. Kondev, M. Hussain *et al.*, Reference cross sections for charged-particle monitor reactions, Nucl. Data Sheets **148**, 338 (2018).

[6] G. W Severin, J. W Engle, T. E Barnhart, and R. J. Nickles, ^{89}Zr radiochemistry for positron emission tomography, Med. Chem. **7**, 389 (2011).

[7] F. Ditrói, A. Hermanne, E. Corniani, S. Takács, F. Tárkányi, J. Csikai, and Y. N. Shubin, Investigation of proton induced reactions on niobium at low and medium energies, Nucl. Instrum. Methods Phys. Res. Sect. B **267**, 3364 (2009).

[8] B. Lawriniang, R. Ghosh, S. Badwar, V. Vansola, Y. S. Sheela, S. Suryanarayana, H. Naik, Y. Naik, and B. Jyrwa, Measurement of cross-sections for the ^{93}Nb(p,n)^{93m}Mo and ^{93}Nb(p,pn)^{92m}Nb reactions up to ≈20 MeV energy, Nucl. Phys. A **973**, 79 (2018).

[9] S. Parashari, S. Mukherjee, B. Nayak, R. Makwana, S. Suryanarayana, H. Naik, and S. Sharma, Excitation functions of the $p + {}^{93}$Nb reaction in the energy range 10–22 MeV, Nucl. Phys. A **978**, 160 (2018).

[10] I. Rizvi, K. Kumar, T. Ahmad, A. Agarwal, and A. Chaubey, Energy dependence of pre-equilibrium emission for the (p, xn) reactions in niobium, Indian J. Phys. **86**, 913 (2012).

[11] Y. E. Titarenko, V. Batyaev, A. Y. Titarenko, M. Butko, K. Pavlov, S. Florya, R. Tikhonov, V. Zhivun, A. Ignatyuk, S.

Mashnik *et al.*, Measurement and simulation of the cross sections for nuclide production in ^{93}Nb and ^{nat}Ni targets irradiated with 0.04-to 2.6-GeV protons, Phys. At. Nucl. **74**, 537 (2011).

[12] G. Steyn, C. Vermeulen, F. Szelecsenyi, Z. Kovacs, K. Suzuki, T. Fukumura, and K. Nagatsu, Excitation functions of proton induced reactions on ^{89}Y and ^{93}Nb with emphasis on the production of selected radio-zirconiums, J. Korean Phys. Soc. **59**, 1991 (2011).

[13] M. Avila-Rodriguez, J. Wilson, M. Schueller, and S. McQuarrie, Measurement of the activation cross section for the (p,xn) reactions in niobium with potential applications as monitor reactions, Nucl. Instrum. Methods Phys. Res. Sect. B **266**, 3353 (2008).

[14] R. Michel, R. Bodemann, H. Busemann, R. Daunke, M. Gloris, H.-J. Lange, B. Klug, A. Krins, I. Leya, M. Lüpke *et al.*, Cross sections for the production of residual nuclides by low-and medium-energy protons from the target elements C, N, O, Mg, Al, Si, Ca, Ti, V, Mn, Fe, Co, Ni, Cu, Sr, Y, Zr, Nb, Ba and Au, Nucl. Instrum. Methods Phys. Res. Sect. B **129**, 153 (1997).

[15] V. Levkovski, Cross sections of medium mass nuclide activation (A = 40–100) by medium energy protons and alpha particles (E = 10–50 MeV), Thesis, Moscow, USSR (1991).

[16] B. G. Kiselev and N. R. Fajzrakhmanova, Reaction cross sections of (p, n), (p, pn) and (p, $\alpha + $n) on ^{93}Nb, 24th Conf. on Nucl. Spectr. and Nucl. Struct., Kharkov 1974, USSR, p. 356.

[17] G. Albouy, J. Cohen, M. Gusakow, N. Poffé, H. Sergolle, and L. Valentin, Réactions (p, 3p3n) entre 30 et 150 MeV, J. Phys. Radium **24**, 67 (1963).

[18] L. Mokhtari Oranj, M. Bakhtiari, N. S. Jung, A. Lee, and H. S. Lee, Extension of excitation functions of proton-induced reactions on bismuth, Phys. Rev. C **101**, 014602 (2020).

[19] L. Mokhtari Oranj, N. S. Jung, M. Bakhtiari, A. Lee, and H. S. Lee, Cross sections of proton-induced nuclear reactions on bismuth and lead up to 100 MeV, Phys. Rev. C **95**, 044609 (2017).

[20] A. Koning, S. Hilaire, and S. Goriely, User Manual of TALYS-1.95, http://www.talys.eu/download-talys/

[21] A. Koning, D. Rochman, J.-C. Sublet, N. Dzysiuk, M. Fleming, and S. Van Der Marck, TENDL: Complete nuclear data library for innovative nuclear science and technology, Nucl. Data Sheets **155**, 1 (2019).

[22] S. Hilaire, M. Girod, S. Goriely, and A. J. Koning, Temperature-dependent combinatorial level densities with the D1M Gogny force, Phys. Rev. C **86**, 064317 (2012).

[23] J. Luo, L. Jiang, and S. Li, Activation cross section and isomeric cross section ratios for the (n, 2n) reaction on ^{153}Eu, Phys. Rev. C **96**, 044617 (2017).

[24] S. Goriely, S. Hilaire, and A. J. Koning, Improved microscopic nuclear level densities within the Hartree-Fock-Bogoliubov plus combinatorial method, Phys. Rev. C **78**, 064307 (2008).

[25] L. M. Oranj, N. S. Jung, J. H. Oh, and H. S. Lee, 100-MeV proton beam intensity measurement by Au activation analysis using ^{197}Au(p, pn)^{196}Au and ^{197}Au (p, p3n)^{194}Au reactions, Nucl. Instrum. Methods Phys. Res. Sect. B **375**, 26 (2016).

[26] Goodfellow, www.goodfellow.com.

[27] J. F. Ziegler, M. Ziegler, and J. Biersack, Srim–the stopping and range of ions in matter (2010), Nucl. Instrum. Methods Phys. Res. Sect. B **268**, 1818 (2010).

[28] Genie 2000 basic spectroscopy software, version 3.2, www.Canberra.com.

[29] Y. E. Titarenko, S. P. Borovlev, M. A. Butko, V. M. Zhivun, K. V. Pavlov, V. I. Rogov, A. Y. Titarenko, R. S. Tikhonov, S. N. Florya, and A. B. Koldobskiy, Cross sections for monitor reactions ^{27}Al(p, x)^{24}Na, ^{27}Al(p, x)^{22}Na, and ^{27}Al(p, x)^{7}Be at proton energies in the range 0.04–2.6 GeV, Phys. Atom. Nucl. **74**, 507 (2011).

[30] ENSDF database, http://www.nndc.bnl.gov/ensarchivals/.

[31] A. Gilbert and A. G. W. Cameron, A composite nuclear-level density formula with shell corrections, Can. J. Phys. **43**, 1446 (1965).

[32] W. Dilg, W. Schantl, H. Vonach, and M. Uhl, Level density parameters for the back-shifted fermi gas model in the mass range 40 < A < 250, Nucl. Phys. A **217**, 269 (1973).

[33] A. Koning and J. Delaroche, Local and global nucleon optical models from 1 keV to 200 MeV, Nucl. Phys. A **713**, 231 (2003).

[34] J. Kopecky and M. Uhl, Test of gamma-ray strength functions in nuclear reaction model calculations, Phys. Rev. C **41**, 1941 (1990).

[35] A. Spyrou, A. Lagoyannis, P. Demetriou, S. Harissopulos, and H.-W. Becker, Cross section measurements of (p, γ) reactions on Pd isotopes relevant to the p process, Phys. Rev. C **77**, 065801 (2008).

[36] S. Harissopulos, A. Spyrou, V. Foteinou, M. Axiotis, G. Provatas, and P. Demetriou, Systematic study of proton capture reactions in medium-mass nuclei relevant to the p process: The case of ^{103}Rh and ^{113,115}In, Phys. Rev. C **93**, 025804 (2016).

[37] E. Bauge, J. P. Delaroche, and M. Girod, Lane-consistent, semimicroscopic nucleon-nucleus optical model, Phys. Rev. C **63**, 024607 (2001).

[38] W. Hauser and H. Feshbach, The inelastic scattering of neutrons, Phys. Rev. **87**, 366 (1952).

[39] M. Bakhtiari, M. Sadeghi, M. K. Bakht, and H. Ghafoori-Fard, Nuclear model calculations of charged-particle-induced reaction cross section data for the production of the radiohalogen ^{34}Cl^{m}, Phys. Rev. C **87**, 034621 (2013).

[40] M. Sadeghi, M. Bakhtiari, M. K. Bakht, M. Anjomrouz, and L. Mokhtari, Overview of mercury radionuclides and nuclear model calculations of ^{195}Hg^{m,g} and ^{197}Hg^{m,g} to evaluate experimental cross section data, Phys. Rev. C **85**, 034605 (2012).

[41] S. Goriely, F. Tondeur, and J. Pearson, A Hartree–Fock nuclear mass table, At. Data Nucl. Data Tables **77**, 311 (2001).

[42] A. V. Ignatyuk, J. L. Weil, S. Raman, and S. Kahane, Density of discrete levels in ^{116}Sn, Phys. Rev. C **47**, 1504 (1993).

[43] P. Demetriou, C. Dufauquez, Y. El Masri, and A. J. Koning, Light charged-particle production from proton- and α-induced reactions on ^{nat}Si at energies from 25 to 65 MeV: A theoretical analysis, Phys. Rev. C **72**, 034607 (2005).

[44] A. Koning and M. Duijvestijn, A global pre-equilibrium analysis from 7 to 200 MeV based on the optical model potential, Nucl. Phys. A **744**, 15 (2004).